Hindawi
Shock and Vibration
Volume 2021, Article ID 5829239, 15 pages
https://doi.org/10.1155/2021/5829239

Research Article

The Impact Behavior between Coal Gangue Particles and the Tail Beam Based on Rock Failure

Zhengyuan Xin,[1] Qingliang Zeng,[1,2] and Yang Yang[1]

[1]*College of Mechanical and Electronic Engineering, Shandong University of Science and Technology, Qingdao 266590, China*
[2]*College of Information Science and Engineering, Shandong Normal University, Jinan 250358, China*

Correspondence should be addressed to Qingliang Zeng; qlzeng@sdust.edu.cn

Received 19 June 2021; Accepted 18 October 2021; Published 23 November 2021

Academic Editor: Vasudevan Rajamohan

In top coal caving mining, common impact occurs between coal gangue particles and tail beam. Little attention has been paid to the effects of coal gangue particles failure on impact force and tail beam response theoretically, numerically, and experimentally. This paper aims to reveal the influence of coal gangue particles failure on the impact effect of tail beam. First, this paper incorporates the theory of rock failure and energy consumption to assess the impact process of coal gangue particles on the tail beam. A new model to simulate the actual failure conditions of rock particles was developed: the brittle damage-fracture particle model. By comparing damage phenomena and simulation data, the brittle damage-fracture particle model was proved to be correct. Based on this model, a dynamic simulation of brittle coal gangue particles impacting the tail beam was conducted. Then, the dynamic responses of the particles and tail beam were analyzed. The results show that particle failure significantly affects the impact force and dynamic response of the tail beam. The impact effects of coal and gangue particles on the tail beam and their failure energy consumption also differed significantly. This paper stresses the importance of coal gangue particle failure conditions for research on top coal caving mining. Theoretical support is provided for the research of coal gangue identification technology based on the tail beam vibration signal.

1. Introduction

In top coal caving, the intelligent identification method of coal and gangue has always been the focus of scholars across the world. Based on tail beam vibrations caused by the impact of coal gangue, coal gangue identification technology detects the vibration signal of the tail beam and identifies the degree of top coal caving, which offers good development prospect [1–4]. In the top coal caving process, as shown in Figure 1, coal gangue particles pass through both shield beam and tail beam and then fall on the scraper conveyor [5–9]. In this process, both coal and gangue particles will collide with each other and with the hydraulic support. Because of the brittleness of coal gangue particles and the natural cracks these contain, when coal gangue particles collide with the tail beam of the hydraulic support, they usually fail. In the process of top coal caving, a large volume of coal gangue will be broken. This will cause a significant difference between the actual vibration signal of the tail beam and the theoretical vibration signal. This in turn can lead to coal gangue identification errors. This problem has been ignored by most scholars. Therefore, it is important to study the mechanism of coal gangue particle impact failure, the effects of particle failure on impact force, and the response of the tail beam.

A number of scholars have attempted to simulate rock impact effects and have investigated the rock fracture mechanism. An and Tannant [10] developed a discrete element contact model for an inelastic rock shock dynamics simulation. Vu-Quoc et al. [11, 12] presented an elastoplastic frictional tangential force displacement (TFD) model for spheres in contact for accurate and efficient granular-flow simulations. Stronge and Ashcroft [13] studied a planar theory for oblique impact of thin-walled spherical balls against a rough rigid surface. Wang et al. [14] focus on the contact problem of a rigid sphere sliding on a layered half-

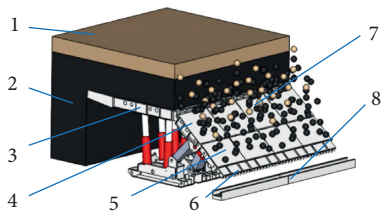

Figure 1: Top coal caving. 1. Coal-gangue mixture seam; 2. Thick seam; 3. Top beam; 4. Shield beam; 5. Tail beam; 6. Poling plate; 7. Coal guage particles; 8. Scraper conveyor.

space with a spring-like interface between the layer and the substrate. Brizmer et al. [15] studied the fundamental problem of elastic-plastic normally loaded contact between a deformable sphere and a rigid flat. Yang et al. [16] proposed a new dimensionless parameter Omega and established the mass-spring-damped oscillator model (MSDOM) and the new contact theory with the consideration of the sphere mass and Omega. These scholars assumed that the rock was either elastic or plastic, without considering rock failure. An elastoplastic model is only suitable for simulations of elastic collisions, but not for rocks with brittle properties. Therefore, it is still difficult to conclude the effects of the failure of a falling rock on the impact force and response of the tail beam. Vervoort et al. [17] studied the behavior of transversely isotropic rock material under Brazilian test conditions for nine different rocks. Yang et al. [18] used the particle flow modeling method to investigate the failure mechanism of transversely isotropic rocks subject to uniaxial compressive loading. Wen et al. [19] conducted a brittleness evaluation based on the energy evolution during rock failure. Gui et al. [20] used the continuous-discrete mixed element method to simulate the dynamic failure of brittle rocks. These scholars conducted detailed studies on the dynamics of rock failure but have not considered the natural cracks in the rock itself. Zou and Wong [21] did the research of cracking processes in a natural rock that is extended to dynamic loading conditions, which are then compared with the quasistatic results. Zhou et al. [22] used acoustic emission (AE) measuring and photographic monitoring techniques to analyze the relationships between the stress, AE, and crack evolution process. Sharafisafa and Shen [23] carried out experimental study on the dynamic fracture behavior of 3D printed rock-like disc specimens with various preexisting flaw configurations under high strain rate loading. However, these studies are limited to the artificial addition of regular cracks, which cannot represent the random fracture of natural rocks. Furthermore, the current research identified the failure of rocks as significantly important and complicated factors, which should be investigated more systematically.

When studying coal gangue failure mechanisms, on the one hand, compared with experimental investigations, simulations can more directly obtain the energy conversion in the particle failure process. On the other hand, in top coal caving mining, the particles contain many cracks or microcracks. Such a state cannot be easily realized experimentally. Therefore, it is particularly important to establish a simulation model that can simulate natural rock damage conditions.

Based on the above reasons, this study used Abaqus numerical analysis software to simulate the process. The damage effect of the impacted part of the rock was simulated by setting the brittle cracking function and the element failure deletion function. Furthermore, zero-thickness vulnerable elements were inserted between ordinary elements to simulate microcracks inside the rock. This simulates the real rock random fracture conditions to the greatest extent. The brittle damage-fracture particle model was obtained and validated via test data and comparative analysis. In contrast to the traditional preset cracks, because there are vulnerable elements in each element in the model, the expansion of the connection between them is completely random. The model will produce completely different cracks because of the different forces. Based on the results, the difference of the tail beam impacted by brittle coal gangue particles was further studied, which provides theoretical support for the realization of coal gangue identification technology based on tail beam vibration signals.

The innovations and main contributions of this paper are described as follows.

(1) Based on the Bond and Holmes theory, this paper conducted a detailed study on the theory of energy consumption theory of rock failure and its impact failure mechanism

(2) A new method is proposed to simulate microcracks inside the rock by inserting zero-thickness vulnerable elements

(3) A new rock failure model is established: the brittle damage-fracture particle model, which can simulate the real rock random fracture conditions to the greatest extent

(4) Comprehensive experiments and simulations are designed and executed to comprehensively prove the effectiveness of the new model

(5) Based on the above model, this paper simulated the impact of coal gangue particles on the tail beam and discussed the feasibility of coal gangue identification technology based on the tail beam vibration signal

2. Energy Consumption Theory of Rock Failure and Its Impact Failure Mechanism

As shown in Figure 2, when coal gangue particles collide with the tail beam, part of the kinetic energy they carry is used for particle failure. The remaining part acts on the tail beam, which causes tail beam vibration. Therefore, exploration of coal gangue particle failure energy consumption and its impact failure mechanism is of great significance for coal gangue identification technology based on tail beam vibration signals.

2.1. Theory of Failure Energy Consumption. In 1867, Rittinger [24] proposed the area theory; that is, the energy consumption of crushing is directly proportional to the

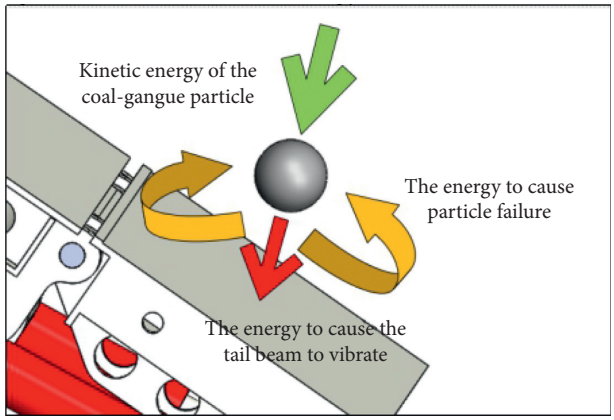

Figure 2: Energy change of coal gangue particle impacting the tail beam.

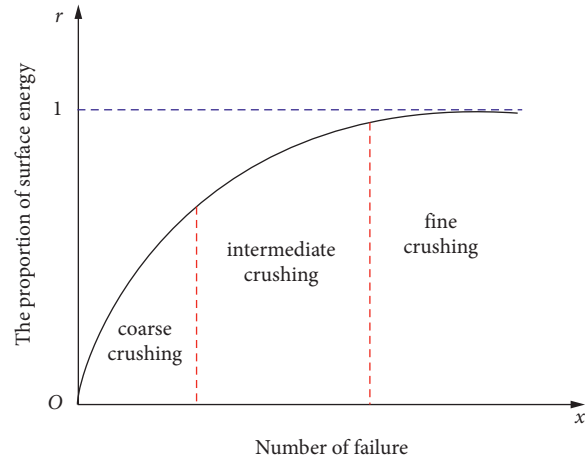

Figure 3: Changing curve of surface energy percentage.

surface area of the new generation during crushing. In 1885, Kick [24] proposed the volume theory, in which crushing energy consumption is proportional to the increment of deformation volume. In fact, the crushing energy consumption is due to the deformation of materials on the one hand and the cohesion of materials on the other hand. Kick only considers the former, and Rittinger only considers the latter. Therefore, in 1951, Bond proposed the famous crack theory.

According to the crack theory proposed by Bond [25–28], the energy consumed during rock fragmentation can be divided into deformation energy and surface energy. The rock failure energy is transformed from deformation energy to surface energy. According to the theory of Holmes [29], rock ore represents nonuniform solids with cracks and other deficiencies. When the applied stress does not reach its theoretical strength, failure will occur. According to the size effect of brittle materials, the energy required to crush rock ore with diameter D can be calculated according to the following equation [29]:

$$E = KD^{1-r}, \tag{1}$$

where K represents the coefficient of deformation energy and r represents the proportion of surface energy in total energy consumption $(0 \le r < 1)$.

Suppose that in continual failure for x times each reduction ratio is 2 and the total reduction ratio is R. The total reduction ratio of x times of failure is $R = 2^x$ or $x = (\lg R/\lg 2)$. The feed diameter of the x^{th} failure is $(D/2^{x-1})$. The value of r is a changing function that gradually approaches 1 with the number of failure x. This trend can be depicted as shown in Figure 3. Among them, the particle size of the coarse crushing stage is about 100–550 mm, the particle size of the intermediate crushing stage is 20–100 mm, and the particle size of the fine crushing stage is about 5–15 mm.

If the particle is regarded as a cube, the energy required to split the particle in three directions is $K(D/2^{x-1})^{1-r} \times 3(D/2^{x-1})^2$. Let $r = f(x)$; then, the total energy needed for x times of failure is

$$\begin{aligned} U &= \sum_{x=1}^{x=(\lg R/\lg 2)} \sum_{r=0}^{r=f(x)} 2^{3(x-1)} \times K\left(\frac{D}{2^{x-1}}\right)^{1-r} \times 3\left(\frac{D}{2^{x-1}}\right)^2 \\ &= 3KD^{3-r} \sum_{x=1}^{x=(\lg R/\lg 2)} \sum_{r=0}^{r=f(x)} 2^{(x-1)r}. \end{aligned} \tag{2}$$

Among them,

$$\sum_{x=1}^{x=(\lg R/\lg 2)} 2^{(x-1)r} = \frac{1-(2^r)^x}{1-2^x} = \frac{1-(2^r)^{\lg R/\lg 2}}{1-2^r} = \frac{R^r-1}{2^r-1}. \tag{3}$$

And so,

$$U = \sum_{r=0}^{r=f(x)} \frac{3KD^{3-r}(R^r-1)}{2^r-1}. \tag{4}$$

It can be seen from (4) that the energy consumed by rock failure is positively related to the diameter D of the rock and its failure degree.

According to the relationship between energy and product particle size as proposed by Hukki [30, 31], the energy-particle size curve is shown in Figure 4. The smaller the particle size in the same rock failure process, the larger the energy required to achieve failure. $r = 0$ implies that only deformation energy exists, which is the elastic deformation stage of the rock. $0 < r < 1$ represents rock failure, where the deformation energy is gradually transformed into surface energy. $r \ge 1$ represents the theoretically possible plastic deformation stage because the particle size of the rock is too small and no longer causes failure.

2.2. Coal Gangue Particle Failure Mechanisms. When the rock is subject to impact, the external force first deforms the rock, and the rock stores deformation energy. When the change reaches a critical point, cracks appear, and multiple cracks expand and connect. The stored deformation energy is then released and converted into surface energy, which leads to the generation of new surfaces. Therefore,

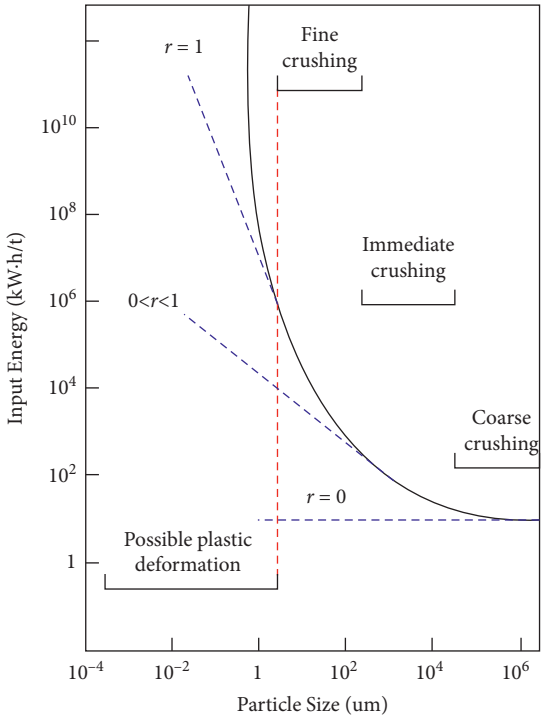

Figure 4: Energy-particle size curve.

deformation energy and surface energy should mainly be considered in the rock failure process.

Rock failure by impact can be divided into two types according to the location and degree of failure: "damage" when only the impacted part is affected and "fracture" when the whole rock block is affected. First, damage is caused when the external force on the impacted part of the rock exceeds the shatter strength of the rock itself. In the process when coal gangue impacts the tail beam, this phenomenon occurs at the position where gangue particles impact the tail beam. Fracture happens because of naturally formed cracks on the surface and within the rocks and ore, as shown in Figure 5. When rock with cracks is subjected to the external force, even if this external force does not reach the shatter strength of the rock, natural cracks will still expand and connect, thus causing complete rock fracture. A schematic diagram of coal gangue particles impacting the tail beam and causing fracture is shown in Figure 6. Coal gangue particles are impacted, and microcracks appear in the particles under the action of external force. These cracks connect with existing cracks, which eventually fractures gangue particles.

Therefore, in dynamic simulations of the impact of coal gangue particles on the tail beam, it is necessary to simulate not only the damage of the impact part of the particles, but also the fracture of the particle as a whole.

3. Establishment of the Simulation Model and Selection of the Particle Damage Model

3.1. Establishment of a Simplified Model and Its Mesh Division. To simulate coal gangue particles impacting the tail beam, the hydraulic support was modeled according to the size of

Figure 5: Cracks in the rock.

the ZF5600/16.5/26 type top coal caving hydraulic support. Since the focus of this study was on how coal gangue particles impact the tail beam and the top beam, the base and the Jack between both do not have direct contact with the tail beam; therefore, many simulation calculations were unnecessary. To decrease the time required for calculation without changing the position of the hinge points of the hydraulic support, the base, top beam, and other parts that are only supporting and not in direct contact with the tail beam are simplified. Since the existence of the insert plate has no impact on the motion state or motion trend of the tail beam, this part is omitted. Figure 7 shows the simplified tail beam model, coal gangue particle model, and its element division. The 3D model of the coal gangue particles impacting the tail beam is built in Abaqus and meshed. The rock sphere is freely meshed via the mesh generation function of ABAQUS. The element size is 0.0015 m, totaling 7,936 elements. A hexahedral element can promote the calculation accuracy. However, the size of the tail beam is large (about 0.5–0.7 m^3) and the structure of the box body is complicated. If all tail beams are divided into hexahedral elements, the calculation time will become excessive. Therefore, the metal plate of the overlying strata of the tail beam (which will be impacted and contacted by the rock sphere) is divided into hexahedral elements with an element size of 0.02 m. The rest is meshed freely into tetrahedral elements with an element size of 0.02 m. After the completion of the mesh generation, the tail beam has a total of 65,137 elements. The simulation model is comprised of 546,318 elements.

3.2. Selection of the Properties of Hydraulic Support Materials. Since this paper studies the impact of single particles, the deformation of the tail beam remains within the elastic range. Therefore, the hydraulic support is set as an elastomer in this paper. This study used the "material editor" in Abacus software to assign material properties to simulation models. According to zF5600/16.5/26 type top coal caving hydraulic support, the support structure should be built with high strength steels such as Q345, Q460, and Q550 (the yield strength of these steels is 345 Mpa, 460 Mpa, and 550 Mpa, resp.) [32]. All three materials meet the strength

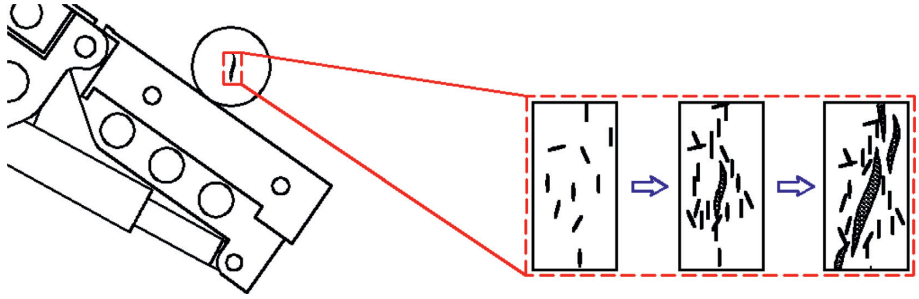

Figure 6: Fracture process of coal gangue particle.

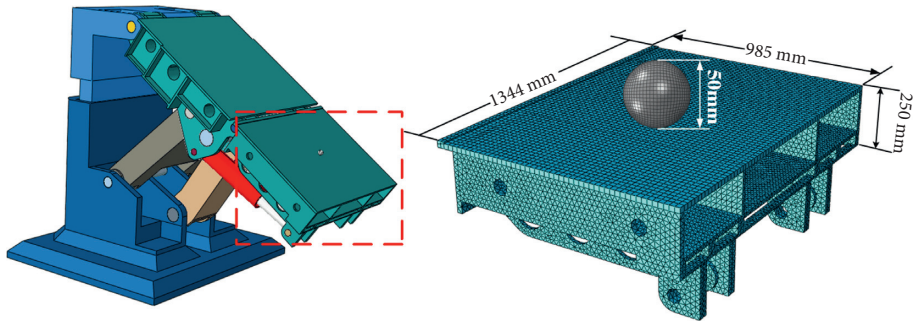

Figure 7: Simplified model of hydraulic support and meshing of tail beam and particles.

requirements of the model. Although the strength of Q460 and Q550 exceeds that of Q345, their weldability is lower because of their increased carbon equivalent. Therefore, to ensure both strength and weldability of steel at the same time, this paper chose Q345 steel as material in the tail beam model.

The hydraulic cylinder part is always built by steel with high strength and hardness such as 35# and 45# (the carbon content of these steels is 0.35% and 0.45%, resp.) [32]. Because both strength and hardness of 45# steel exceed those of 35# steel, 45# steel was chosen for the hydraulic cylinder part. Material features are listed in Table 1.

3.3. The Establishment of Particle Simulation Models and Their Comparative Analysis through Impact Phenomena of Particles. To simulate the actual rock failure phenomenon to the maximum extent, three different particle models were set up. By comparing the impact phenomenon of these three models with that of coal gangue in the experiment, the closest particle simulation model to the actual damage situation is obtained.

3.3.1. Traditional Particle Models. According to the ideas proposed by Yang et al. [16], this study first built Model 1 (i.e., the elastic particle model). To achieve the crushing effect of the particle model, the method of simulating material damage by Lu et al. [33] was applied. The brittle cracking function and the element failure deletion function were used in the material editor of Abaqus to obtain Model 2 (i.e., the brittle damage particle model).

Table 1: Main material properties of steels.

Material	Density ($kg \cdot m^{-3}$)	Elastic modulus (Pa)	Poisson's ratio
Q345	7850	2.06×10^{11}	0.3
45	7890	2.09×10^{11}	0.269

When Model 1and Model 2 are used to simulate the impact tail beam, the effect is shown in Figures 8 and 9. Figure 8(a) shows the state of Model 1 after it impacts the tail beam. Because this particle model is an elastomer, it will not be damaged at all. Figures 8(b)–8(d) show the process of Model 1 impacting the tail beam. Figure 8(b) shows the state of the particle before it collides with the plane. In Figure 8(c), the particle collides with the plane and elastic deformation occurs at the particle contact position. In Figure 8(d), after the particle collision, the elastic deformation recovered to its original state. This model is only applicable to the analysis of regularity, but not that of rock particle damage. When a particle impacts the tail beam, the part in contact with the tail beam fails because of the force. Therefore, it is deleted to simulate local damage of the particle. Figure 9(a) shows the state of Model 2 after impacts on the tail beam. Figures 9(b)–9(d) show the process of Model 2 impacting the tail beam. In Figure 9(c), the particle contacts the plane and the contact part begins to be damaged. In Figure 9(d), the impact ended without particle bouncing. Only the lower part of the particle is damaged because of its impact with the tail beam. Because the crushing phenomenon of Model 2 is achieved simply through the deletion of units, it cannot correctly simulate the fracture of rocks. Therefore, this model is not suitable for the simulation of rock damage.

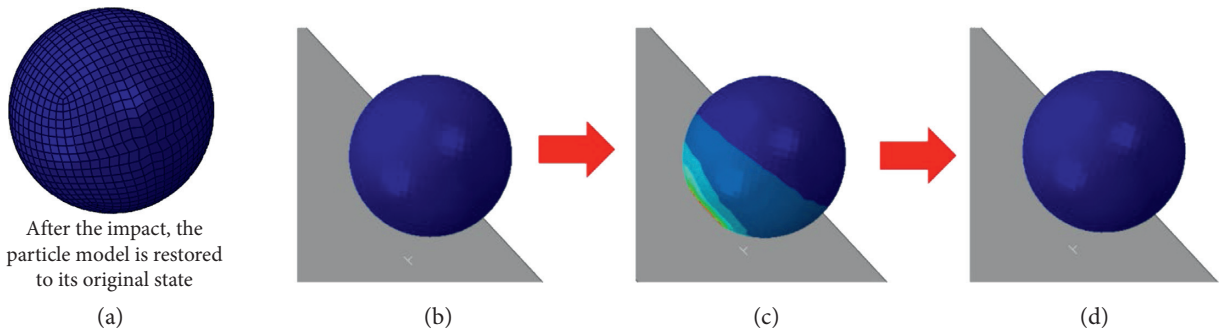

Figure 8: Impact effect diagram of Model 1.

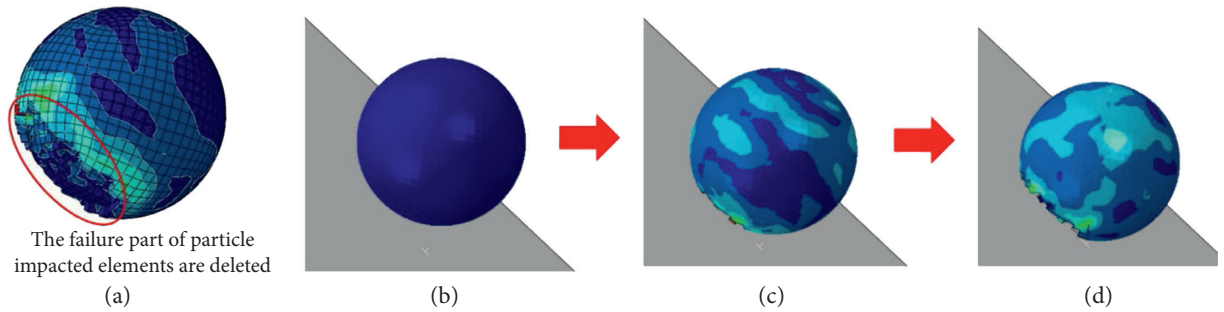

Figure 9: Impact effect diagram of Model 2.

3.3.2. Brittle Damage-Fracture Particle Model. To further simulate the fracture of particles with microcracks during the impact process, this simulation inserts zero-thickness vulnerable elements between normal elements to simulate cracks. At the same time, to ensure the randomness of crack expansion, zero-thickness vulnerable elements are inserted between all elements of the particle model, as shown in Figure 10.

Figure 10(a) shows the zero-thickness element that is inserted between two adjacent elements. Figure 10(b) shows the state of the particle model after all elements were inserted into the zero-thickness elements. This is equal to microcracks in the rock. These vulnerable elements will break first when the model is impacted. In contrast to the traditional preset cracks, because there are vulnerable elements in each element in the model, the expansion of the connection between them is completely random. The model will produce completely different cracks because of the different forces. The traditional method of preset cracks only shows cracks at the same location. Model 3 (i.e., the brittle damage-fracture particle model) not only causes local damage but also generates random fracture effects according to the applied force. When this particle model is used to simulate the impact tail beam, the effect is shown in Figure 11.

Figure 11(a) shows the state of Model 3 after it impacts the tail beam. Figures 11(b)–11(d) show the process of Model 3 impacting the tail beam. In Figure 11(a), not only the bottom contact part is damaged, but also the entire particle is fractured. In Figure 11(c), after the particle model contacts the plane, cracks start to appear. In Figure 11(d), after the impact, the particle does not bounce back, and the entire particle fractured.

3.3.3. Experiment of Coal-Gangue Particles Impact Damage Phenomenon and Comparative Analysis with Three Particle Simulation Models. To verify the accuracy of the failure phenomenon, this paper conducted an experiment of falling collision and damage of coal gangue particles. The single particle impact test bed is shown in Figure 12. As shown, the single particle impact test bed is mainly composed of the moving coal dropping device 1, shock Table 2, and supporting portal frame 3. The moving coal dropping device is installed on the supporting portal frame, and the height can be freely adjusted, up to 10 m. The shock table is fixed on the floor. The moving coal dropping device is adjusted to 3 m above the shock table, and the coal gangue particle is put into the moving coal dropping device. The switch is started to let coal gangue particles fall freely and impact the shock table. Then, the damage of coal gangue particles is observed.

The resulting damage phenomenon is shown in Figure 13. Figures 13(a) and 13(b) show the damage of coal and gangue after impact, respectively. Comparison indicates that Model 1 (Figure 9) and Model 2 (Figure 10) are not consistent to the crushing mode of coal and gangue particles. Model 1 was not damaged, while Model 2 was only damaged at its contacted part. Both coal and gangue all showed whole fracture from the contact part, equal to the failure effect of Model 3 in Figure 11. It can be possible to conclude that Model 3 (i.e., the brittle damage-fracture particle model) is

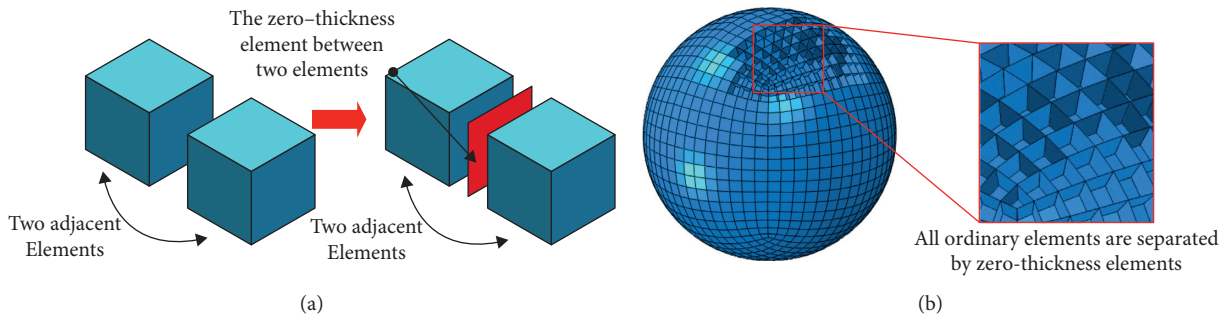

Figure 10: Zero-thickness vulnerable elements.

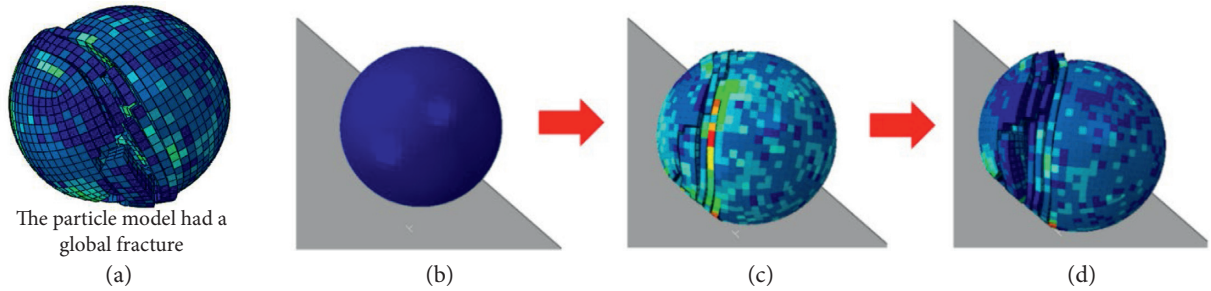

Figure 11: Impact effect diagram of Model 3.

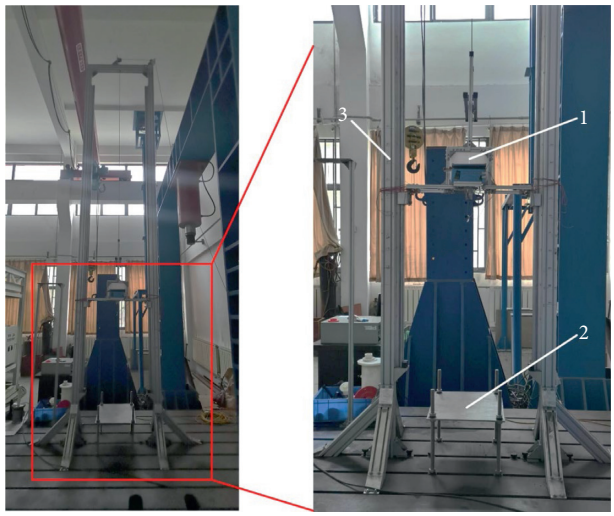

Figure 12: Single particle impact test bed.

most similar to the phenomenon of coal and gangue particle damage. To further discuss the feasibility of Model 3, the impact tail beam on these three models was simulated, and the simulation results were analyzed.

3.4. Comparison Analyses of Three Different Particle Simulation Models through the Simulation Result of the Impact Tail Beam. To further explore the differences between these three model particles during their impact on the tail beam and to discuss the feasibility of Model 3, this study used these three models for numerical simulation.

3.4.1. Setting of Simulation Conditions, Particle Material Properties, and Simulation Jobs. As shown in Figure 14, three types of coal gangue particle models are placed above the center contact point of the tail beam, from where they then fall and impact the tail beam. The supporting height of the top coal caving hydraulic support is about 2.2–4.5 m. In case of free fall, the speed of coal gangue particles hitting the tail beam is about 6–9 m/s. Therefore, to avoid errors in a single simulation result, while ensuring the correctness and universality of all results, impact tail beam dynamics simulation of three particle models was conducted at three different initial velocities ($v = 6$ m/s, 7 m/s, and 8 m/s), which are within the scope of the theory. The particle material is coal. Material features [34] are shown in Table 2. The specific working conditions of the jobs were arranged as shown in Table 3.

3.4.2. Comparative Analysis of Three Particle Simulation Models Impacting the Tail Beam Simulation Results. To explore the impact of the models on the tail beam, the displacement and acceleration vibration curves of the tail beam were extracted at three velocities as shown in Figures 15(a) and 15(b). In Figures 15(a) and 15(b), the acceleration and displacement vibration signals of the tail beam are the strongest under the impact of the elastic particle model and the weakest under the brittle damage-fracture particle model. When the density, elastic modulus, and Poisson's ratio are identical, failure particles have a weaker excitation effect on the tail beam than the elastic particle. This is because the particles need to consume energy to fail, and the greater the degree of

Table 2: Main material properties in particle model.

Material	Density ($kg \cdot m^{-3}$)	Elastic modulus (P)a	Poisson's ratio	Shatter strength (MPa)
Coal (elastic)	1380	2.20×10^9	0.28	—
Coal (brittle)	1380	2.20×10^9	0.28	5
Vulnerable elements	—	—	—	1

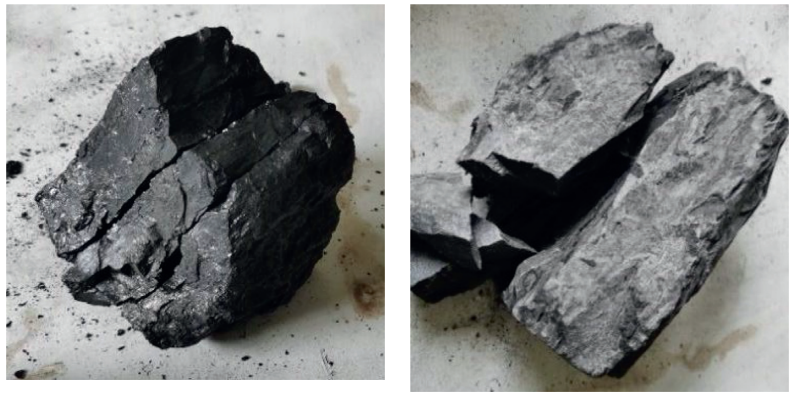

(a) (b)

Figure 13: The phenomenon of coal gangue particle damage.

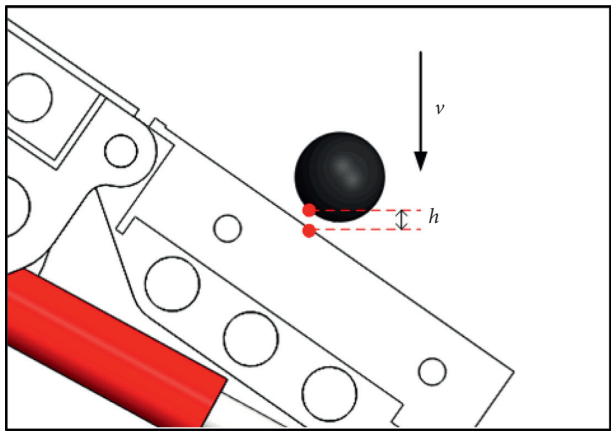

Figure 14: Working condition of coal gangue particles impacting tail beam.

failure is, the more the energy is consumed. Therefore, it is clearly inappropriate to use Model 1 to simulate coal gangue particles. In addition, Model 2 only has partial damage and consumes less energy, which brings the vibration signal of the tail beam close to that of Model 1. Model 3 consumes a lot of energy because of overall fracture; therefore, the vibration signal of the tail beam is significantly smaller than that of both Model 1 and Model 2.

To further explore the differences between these three particle models during their impact on the tail beam and to verify the correctness of Model 3 for shock behavior, the velocity, acceleration, and displacement curves of the particle's center of gravity were extracted at the three velocities. The results are shown in Figures 15(c)–15(e). The elastic particle model is significantly different from the other two brittle models. Its velocity, acceleration, and displacement curves all show apparent and abrupt changes during impact. This is because elastic particles rebound after impacting the tail beam, while brittle particles basically do not rebound but are rather damaged. Since Model 2 can only break a small part and only absorb a small amount of kinetic energy, Figures 15(a) and 15(b) show that it has generated relatively large vibrations. In contrast, Model 3 is completely broken, which can absorb much energy and therefore does not vibrate much. The failure energy consumption of Model 3 is shown in Figure 16.

This section compares the three models in terms of particle signal and tail beam signal and proves that Model 3 can not only simulate the rock breaking phenomenon, but also simulate the working conditions of the rock particle impacting the tail beam.

On the one hand, the damage phenomenon of three kinds of particle simulation models is compared and analyzed based on the experiment of coal gangue particle crushing presented in Section 3.3. On the other hand, the velocity, acceleration, and displacement simulation data were compared between the three kinds of particle simulation models and the tail beam, as shown in Section 3.4. Therefore, based on the above research, Model 3 (i.e., the brittle damage-fracture particle model proposed here) is more suitable to study the impact problem between coal

Table 3: Settings of the simulation jobs.

Jobs	Particle model	Initial speed (m/s)	Particle material
Job1-1	Model 1: elastic particle model	6	Coal (elastic)
Job1-2		7	
Job1-3		8	
Job2-1	Model 2: brittle damage particle model	6	Coal (brittle)
Job2-2		7	
Job2-3		8	
Job3-1	Model 3: brittle damage-fracture particle model	6	Coal (brittle) and vulnerable elements
Job3-2		7	
Job3-3		8	

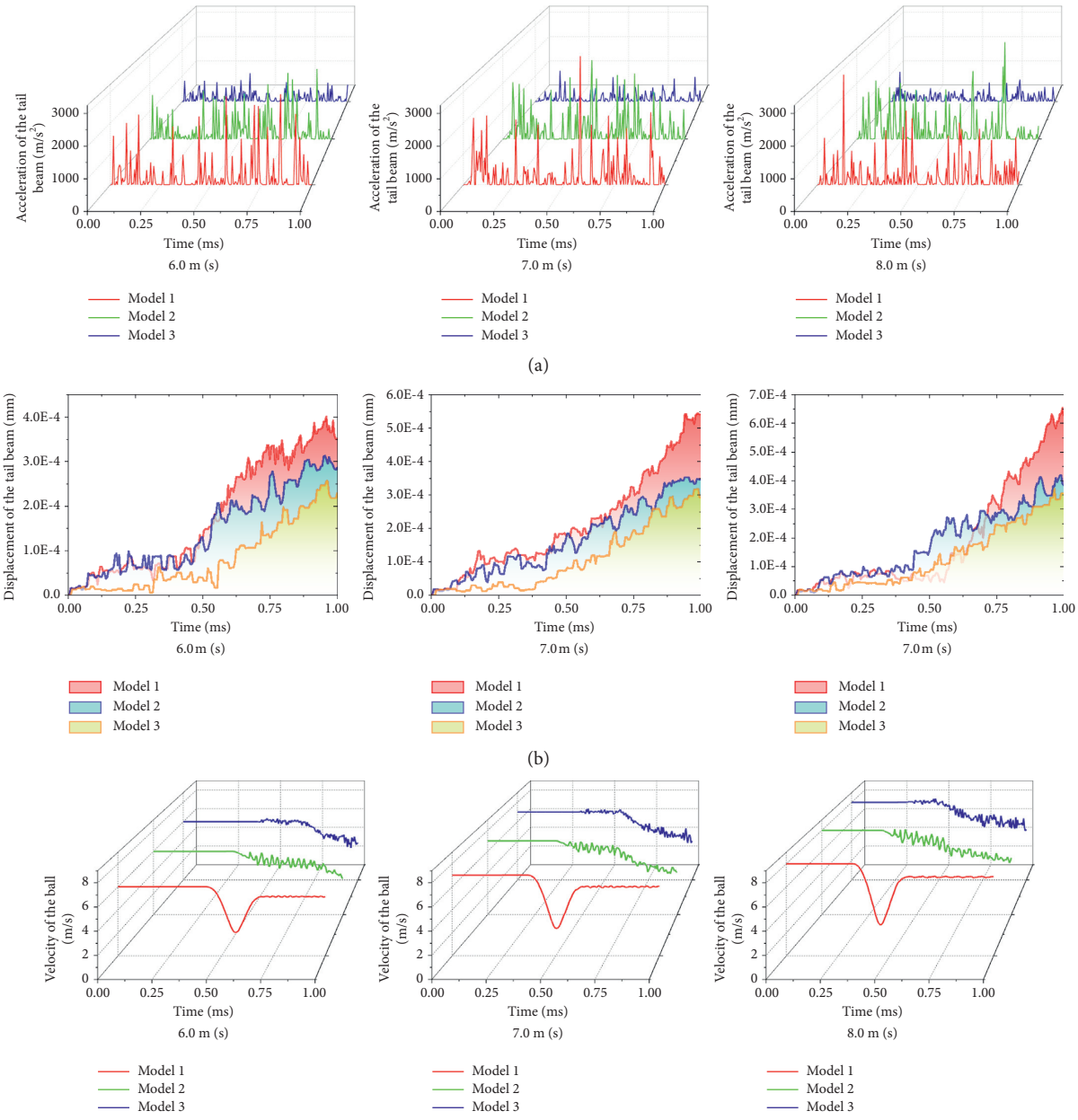

Figure 15: Continued.

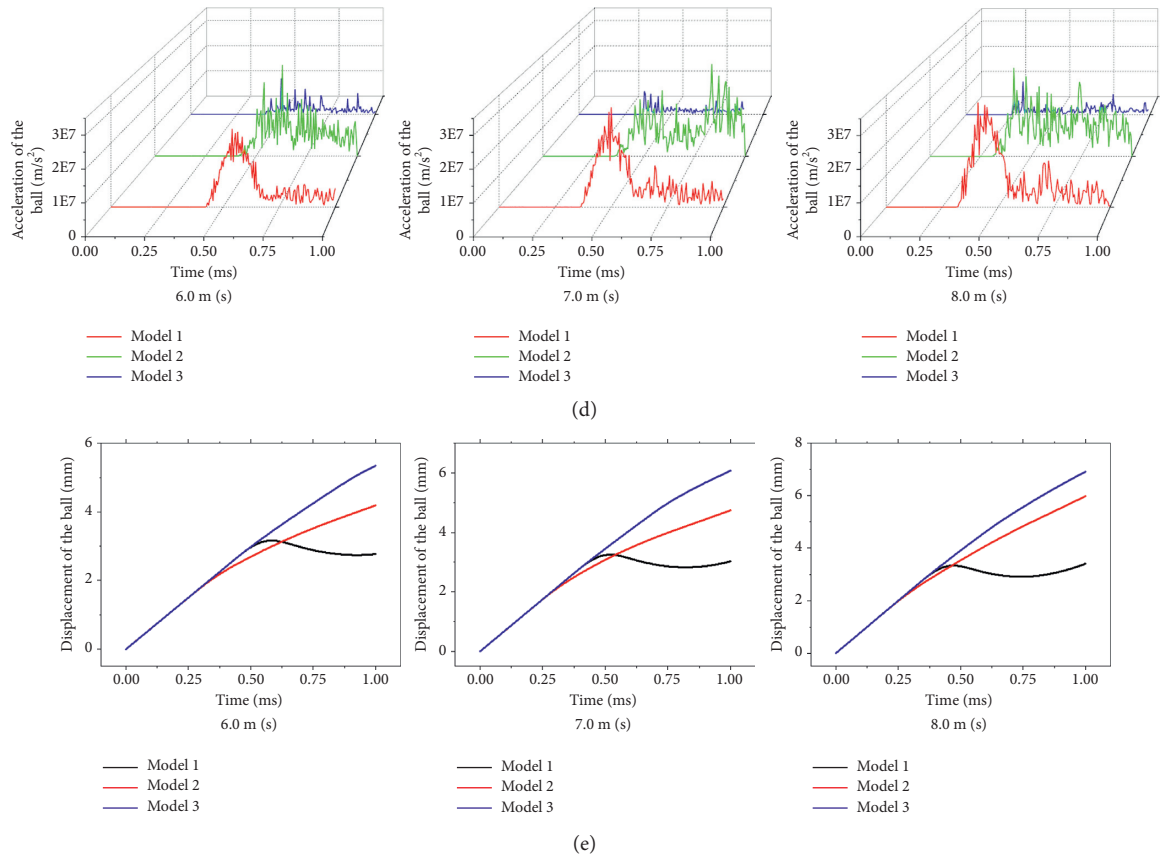

Figure 15: Simulation data. (a) Acceleration of the tail beam. (b) Displacement of the tail beam. (c) Particle velocity. (d) Particle acceleration. (e) Particle displacement.

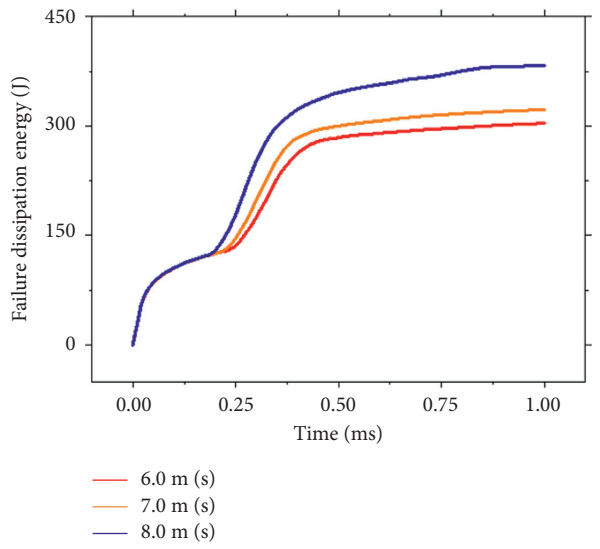

Figure 16: The failure energy consumption of Model 3.

gangue particles and the tail beam. Based on this model, research on the impact behavior between coal gangue particles and the tail beam is presented in the following chapter.

4. Research on the Impact Behavior between Coal Gangue Particles and the Tail Beam Based on the Brittle Damage-Fracture Particle Model

To further explore the impact problem between broken coal gangue particles and the tail beam, based on the brittle damage-fracture particle model developed in the previous section, this section presents a simulation of coal gangue particles impacting the tail beam. Five types of coal and gangue material were selected as model material. The possibility of coal gangue identification technology based on tail beam vibration signal is discussed.

4.1. Setting Up the Simulation Model. Five different coal gangue materials are selected to explore the different effects of coal and gangue impacts on the tail beam.

4.1.1. Material Properties Settings. The material setting of the hydraulic support model remains unchanged. With regard to brittle particles, five different materials were selected: coking coal, anthracite, sandstone, limestone, and marble. The material parameters of vulnerable elements of all models were identical. Material features [34] are shown in Table 4.

Table 4: Material properties of brittle coal gangue particles used in the simulation.

Material	Density ($kg \cdot m^{-3}$)	Elastic modulus (Pa)	Poisson's ratio	Shatter strength (MPa)
Coking coal	1200	2.30×10^9	0.25	5
Anthracite	1600	$4..40 \times 10^9$	0.26	8
Sandstone	2487	1.35×10^{10}	0.123	10
Limestone	2715	4.65×10^{10}	0.26	15
Marble	2800	3.40×10^{10}	0.30	20
Vulnerable element	—	—	—	1

Table 5: Settings of the simulation jobs.

Jobs	Initial speed (m/s)	Particle material
Job-c1-1	6.0	Coking coal
Job-c1-2	7.0	
Job-c1-3	8.0	
Job-c2-1	6.0	Anthracite
Job-c2-2	7.0	
Job-c2-3	8.0	
Job-g1-1	6.0	Sandstone
Job-g1-2	7.0	
Job-g1-3	8.0	
Job-g2-1	6.0	Limestone
Job-g2-2	7.0	
Job-g2-3	8.0	
Job-g3-1	6.0	Marble
Job-g3-2	7.0	
Job-g3-3	8.0	

4.1.2. Simulation Jobs Setting. To ensure accuracy of the simulation, the above five types of coal gangue particles have been dynamically simulated during their impact on the tail beam at three speeds of 6.0 m/s, 7.0 m/s, and 8.0 m/s. The specific working conditions are listed in Table 5.

4.2. Results and Discussion of the Coal Gangue Particle Impact on the Tail Beam. This section discusses the energy consumption differences of coal gangue particles during their impact on the tail beam and the differences in the responses of the tail beam.

4.2.1. Difference Analysis of Failure Energy Consumption and Impact Force. Figures 17(a) and 17(b) show the energy consumed by five types of coal gangue particles during their impact on the tail beam and the impact force on the tail beam for three initial velocities. Figure 17(a) shows that since the deformation energy at the initial stage of failure is dominant during the early stage of particle impact on the tail beam (at about 0–0.25 ms), the shatter strength of the coal sample is smaller than that of the gangue; therefore, it is more easily damaged. Consequently, the failure energy consumption of coal particles is higher than that of gangue particles. At the later stage of failure (at about 0.25–1.00 ms), coal gangue particles are completely fractured. At this time, the surface energy dominates. Because the vulnerable elements of the model are the same, gangue particles with higher kinetic energy are fractured more easily; therefore, the energy consumption of gangue particles is higher than that of coal particles. Figure 17(b) shows that although gangue particles consume more energy when they fail, the density of gangue particles generally exceeds that of coal particles. Consequently, the impact force of gangue particles on the tail beam is significantly higher than that of coal particles.

4.2.2. Difference Analysis of the Impacted Tail Beam Vibration Signal. To further study the difference of the response of the tail beam during impact by coal gangue particles, the speed, acceleration, and displacement vibration signals of the tail beam are extracted. Figures 18(a)–18(c) show the speed, acceleration, and displacement vibration curves of the tail beam, respectively. Unlike the impact effect of elastic particles, brittle fracture particles cause continuous compression on the tail beam; therefore, the vibration signal of the tail beam also has continuous vibration. Figures 18(a)–18(c) show that the vibration signals of the tail beam are similar under the impact of both coal particles. However, because of the large kinetic energy the gangue particles carry, the vibration signal of the tail beam impacted by the gangue particles is significantly higher than that of the tail beam impacted by the coal particles.

In summary, under the premise of brittle coal gangue particle failure, although the gangue of the same volume will consume more kinetic energy, its impact on the tail beam still significantly exceeds that of coal. This causes a stronger impact on the tail beam when the proportion of gangue increases in the coal caving process. Therefore, coal gangue

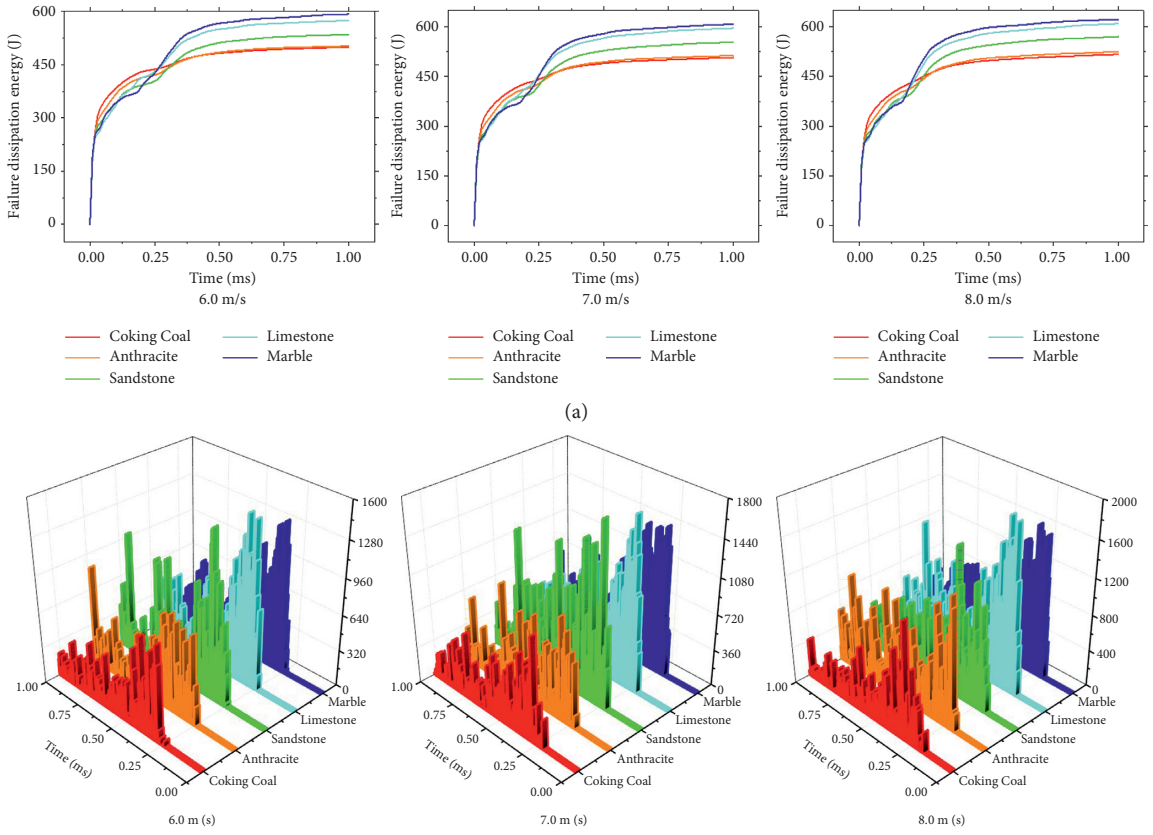

Figure 17: Simulation data of impact process. (a) Energy consumption of coal gangue particle failure. (b) The impact force of coal gangue particles on the tail beam.

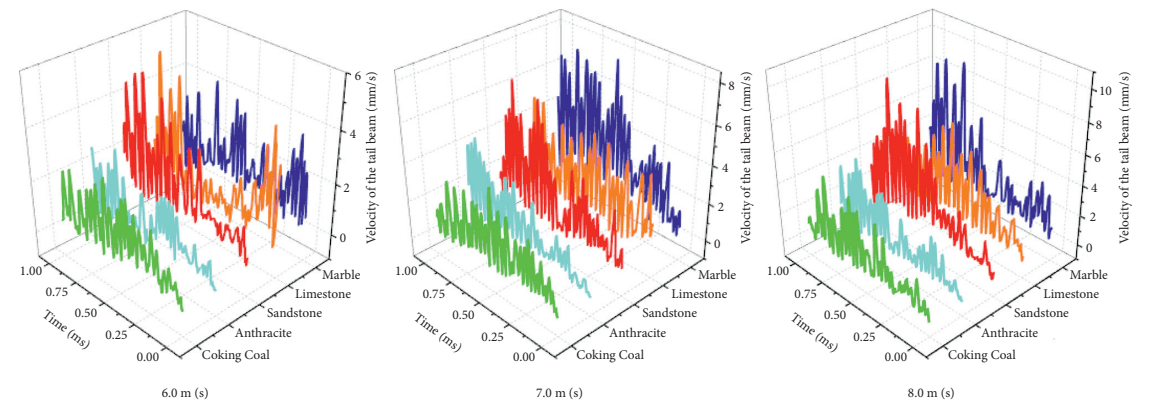

Figure 18: Continued.

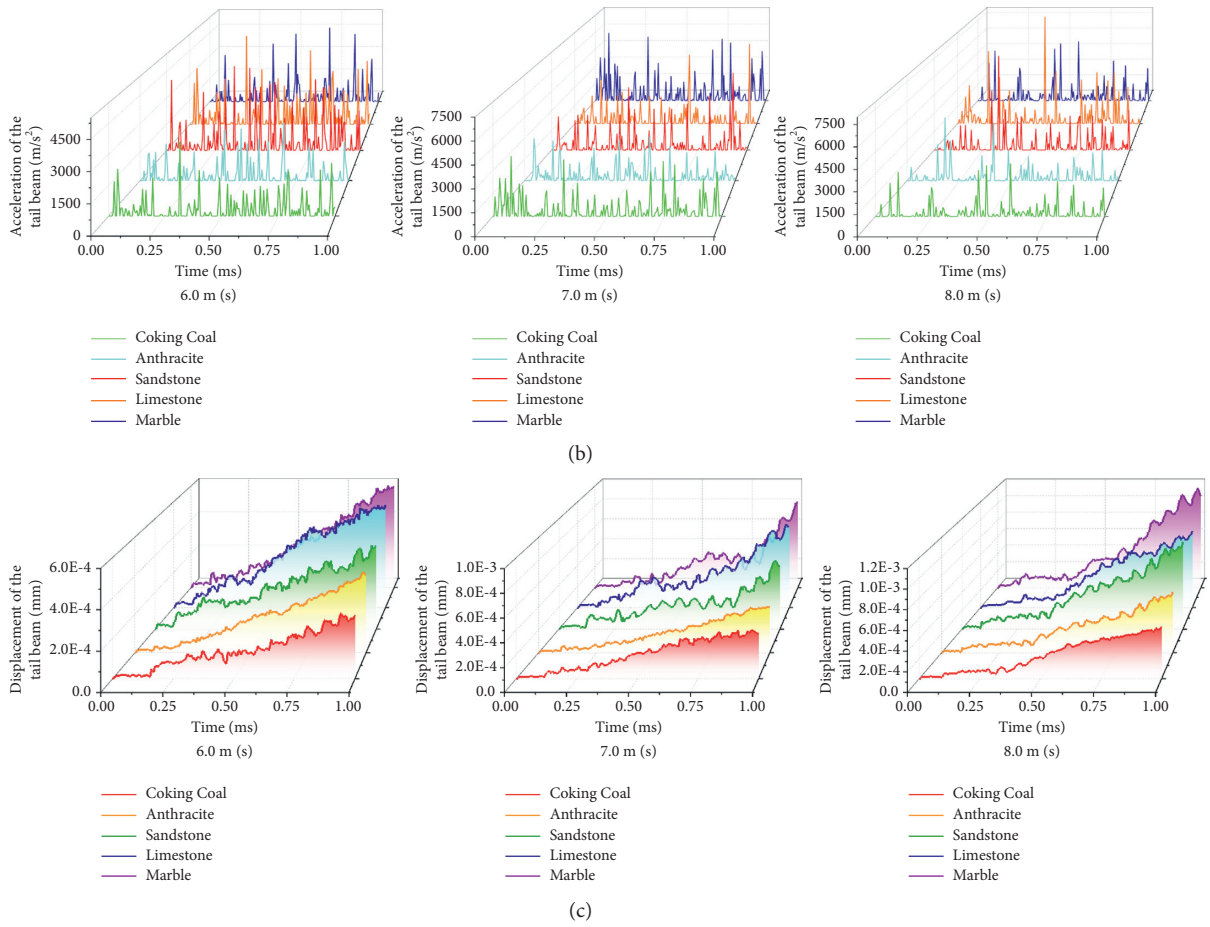

Figure 18: Simulation data of tail beam. (a) Speed vibration signals of tail beam. (b) Acceleration vibration signals of tail beam. (c) Displacement vibration signals of tail beam.

identification technology, based on the tail beam vibration signal, is feasible.

5. Conclusion

In the process of top coal caving, coal gangue particles generally fail when impacting the tail beam. This study investigated the mechanism of coal gangue particle impact failure and its effects on both the impact force and the response of the tail beam. To explore the effect of coal gangue particle failure on the impact force and the response of the tail beam, this study sets up a simplified hydraulic support model and created the brittle damage-fracture particle model for coal gangue particles. Through damage phenomenon and simulation data, the different effects of the three particle models (i.e., elastic particle model, brittle damage particle model, and brittle damage-fracture particle model) were compared and their impacts on the tail beam were assessed. Based on the brittle failure-fracture particle model, dynamic simulations of five types of coal gangue particles impacting the tail beam were conducted. The following conclusions can be drawn from these studies.

(1) Damage of coal gangue particles consumes energy, which affects the impact force. The greater the degree of coal/gangue particle breakage, the greater the energy consumption.

(2) When the coal gangue particles are impacted, the particles should be subject to global fracture because of microcracks in them rather than only at the bottom part damage. This can continue to compress the tail beam rather than only cause instantaneous impact on it.

(3) Comparing the crushing effect of the three particle models and the simulation data of their impact on the tail beam shows that the brittle damage-fracture particle model conforms to the actual situation in terms of both impact and damage effects.

(4) Although the gangue of the same volume will consume more kinetic energy, its impact on the tail beam is still significantly stronger than that of coal because of its greater mass. Therefore, it will cause stronger tail beam vibration. These studies further provide theoretical support for coal gangue identification technology based on the tail beam vibration signal.

The presented research and analysis indicate that the failure of coal gangue particles will consume part of the kinetic energy it carries and the impact effect on the tail

beam will differ. Therefore, when investigating coal gangue identification technology based on tail beam vibration signals, not only the elastic properties of coal gangue particles should be considered, but the failure of coal gangue particles must also be fully considered.

Data Availability

The data used to support the findings of this study are included within the article.

Conflicts of Interest

The authors declare that there are no conflicts of interest regarding the publication of this paper.

Acknowledgments

This work was supported by the National Natural Science Fund of China (51674155 and 51974170), the Innovative Team Development Project of Ministry of Education under Grant IRT_16R45, and the Special Funds for Climbing Project of Taishan Scholars.

References

[1] H. Xie and H. W. Zhou, "Application of fractal theory to top-coal caving," *Chaos, Solitons & Fractals*, vol. 36, no. 4, pp. 797–807, 2008.

[2] F. Simsir and M. K. Ozfirat, "Determination of the most effective longwall equipment combination in longwall top coal caving (LTCC) method by simulation modelling," *International Journal of Rock Mechanics and Mining Sciences*, vol. 45, no. 6, pp. 1015–1023, 2008.

[3] J.-a. Wang, L. Yang, F. Li, and C. Wang, "Force chains in top coal caving mining," *International Journal of Rock Mechanics and Mining Sciences*, vol. 127, Article ID 104218, 2020.

[4] C. Liu, H. Li, and H. Mitri, "Effect of strata conditions on shield pressure and surface subsidence at a longwall top coal caving working face," *Rock Mechanics and Rock Engineering*, vol. 52, 2019.

[5] Z. L. Li, X. Q. He, L. M. Dou, and D. Z. Song, "Comparison of rockburst occurrence during extraction of thick coal seams using top-coal caving versus slicing mining methods," *Canadian Geotechnical Journal*, vol. 55, 2018.

[6] M. Z. Gao, R. Zhang, J. Xie, G. Y. Peng, B. Yu, and P. G. Ranjith, "Field experiments on fracture evolution and correlations between connectivity and abutment pressure under top coal caving conditions," *International Journal of Rock Mechanics and Mining Sciences*, vol. 111, pp. 84–93, 2018.

[7] Z. Zhu, H. Zhang, J. Nemcik, T. Lan, J. Han, and Y. Chen, "Overburden movement characteristics of top-coal caving mining in multi-seam areas," *The Quarterly Journal of Engineering Geology and Hydrogeology*, vol. 51, no. 2, pp. 276–286, 2018.

[8] Y. Z. Wang, B. X. Huang, and S. G. Cao, "Cavability control by hydraulic fracturing for top coal caving in hard thick coal seams," *International Journal of Rock Mechanics and Mining Sciences*, vol. 74, pp. 45–57, 2015.

[9] K. Yang, J. C. Chang, and G. X. Xie, "Investigations into stress shell characteristics of surrounding rock in fully mechanized top-coal caving face," *International Journal of Rock Mechanics and Mining Sciences*, vol. 46, no. 1, pp. 172–181, 2009.

[10] B. An and D. D. Tannant, "Discrete element method contact model for dynamic simulation of inelastic rock impact," *Computers & Geosciences*, vol. 33, no. 4, pp. 513–521, 2007.

[11] L. Vu-Quoc, L. Lesburg, and X. Zhang, "An accurate tangential force-displacement model for granular-flow simulations: c," *Journal of Computational Physics*, vol. 196, no. 1, pp. 298–326, 2004.

[12] L. Vu-Quoc, Z. Xiang, and L. Lesburg, "Normal and tangential force-displacement relations for frictional elasto-plastic contact of spheres," *International Journal of Solids and Structures*, vol. 38, no. 36, pp. 6455–6489, 2001.

[13] W. J. Stronge and A. D. C. Ashcroft, "Oblique impact of inflated balls at large deflections," *International Journal of Impact Engineering*, vol. 34, no. 6, pp. 1003–1019, 2007.

[14] Z. Wang, H. Yu, and Q. Wang, "Layer-substrate system with an imperfectly bonded interface: spring-like condition," *International Journal of Mechanical Sciences*, vol. 134, pp. 315–335, 2017.

[15] V. Brizmer, Y. Kligerman, and I. Etsion, "The effect of contact conditions and material properties on the elasticity terminus of a spherical contact," *International Journal of Solids and Structures*, vol. 43, no. 18-19, pp. 5736–5749, 2006.

[16] Y. Yang, Q. Zeng, L. Wan, L. Wang, and G. Yin, "Research of contact response of an elastic sphere impacting a rigid plate based on the mass-spring-damped oscillator model and dimensionless parameter \omega_\Omega," *International Journal of Acoustics and Vibration*, vol. 25, no. 2, pp. 141–152, 2020.

[17] A. Vervoort, K.-B. Min, H. Konietzky et al., "Failure of transversely isotropic rock under brazilian test conditions," *International Journal of Rock Mechanics and Mining Sciences*, vol. 70, pp. 343–352, 2014.

[18] X. X. Yang, H. W. Jing, and W. G. Qiao, "Numerical investigation of the failure mechanism of transversely isotropic rocks with a particle flow modeling method," *Processes*, vol. 6, 2018.

[19] T. Wen, H. Tang, and Y. Wang, "Brittleness evaluation based on the energy evolution throughout the failure process of rocks," *Journal of Petroleum Science and Engineering*, vol. 194, Article ID 107361, 2020.

[20] Y.-L. Gui, H. H. Bui, J. Kodikara, Q.-B. Zhang, J. Zhao, and T. Rabczuk, "Modelling the dynamic failure of brittle rocks using a hybrid continuum-discrete element method with a mixed-mode cohesive fracture model," *International Journal of Impact Engineering*, vol. 87, pp. 146–155, 2016.

[21] C. Zou and L. N. Y. Wong, "Experimental studies on cracking processes and failure in marble under dynamic loading," *Engineering Geology*, vol. 173, pp. 19–31, 2014.

[22] Z. Zhou, L. Tan, and W. Cao, "Fracture evolution and failure behaviour of marble specimens containing rectangular cavities under uniaxial loading," *Engineering Fracture Mechanics*, vol. 184, 2017.

[23] M. Sharafisafa and L. Shen, "Experimental investigation of dynamic fracture patterns of 3d printed rock-like material under impact with digital image correlation," *Rock Mechanics and Rock Engineering*, vol. 53, no. 7, 2020.

[24] M. U. Fu-Sheng, "Current status and development requirements for the research of theory of comminution," *Sulphur Phosphorus & Bulk Materials Handling Related Engineering*, 2006.

[25] F. C. Bond, "Confirmation of the third theory," *Trans Aime*, vol. 217, 1960.

[26] F. C. Bond, "Crushing tests by pressure and impact," *Trans AIME*, vol. 169, pp. 58–66, 1947.
[27] F. C. Bond, "Crushing and grinding calculations," *Brit.chem.eng*, vol. 47, no. 507, pp. 466–472, 1954.
[28] F. C. Bond, "Crushing and grinding calculations part I," *Brit. chem. eng*, vol. 6, 1961.
[29] J. A. Holms, *Transactions of the Institution of Chemical Engineers*, vol. 35, no. 2, p. 125, 1957.
[30] R. T. Hukki, "Proposal for a solomnic settlement between theories of von rittinger, kick and bond," *Transactions of AIME*, vol. 223, 1962.
[31] R. T. Hukki, "Correlation between principal parameters affecting mechanical ball wear," *Trans. Soc. Miner. Eng. AIME*, vol. 199, pp. 642–644, 1954.
[32] D. X. Cheng, *Handbook of Mechanical Design*, China Machine Press, Beijing, China, 6th edition, 2017.
[33] Z. Lu, L. Wan, Q. Zeng, X. Zhang, and K. Gao, "Numerical simulation of rock plate cutting with three sides fixed and one side free," *Advances in Materials Science and Engineering*, vol. 2018, Article ID 5464295, 21 pages, 2018.
[34] "Editorial board of geological engineering handbook," *Geological Engineering Handbook*, China Architecture & Building Press, Beijing, China, 5th edition, 2018.